ICING AND DE-ICING UNDER CENTRIFIGAL LOADS IN DLR'S WHIRL TOWER FACILITY

Steffen Kalow[1], Rainer Bartels[2], Oliver Schneider[2], Dominic Sahyoun[1], Ralf Keimer[1]

[1] *Institute of Lightweight Systems*, [2] *Institute of Flight Systems*

German Aerospace Center (DLR), 38108 Braunschweig, Germany

Abstract

The paper presents current DLR activities focusing on experimental icing investigations within the InTEnt-H project. The aim of the project is to investigate innovative de-icing and anti-icing technologies for small and medium-weight helicopters, for which no such technologies exist to date, and to demonstrate the effectiveness of these systems in a suitable test facility. For this purpose, the rotor test facility at DLR in Brunswick will be converted into an icing facility that is unique in Europe and will allow the generation of atmospheric icing conditions in compliance with EASA requirements. Furthermore, the progress of the first test campaign of the project will be reported. The focus will be on the first icing tests as well as on the de-icing of a rotating demonstration blade by means of electrically operated heating foils and a waste-heat technology.

1. INTRODUCTION

The development of efficient rotor blade de-icing and anti-icing technologies for helicopters is a major challenge. For today's large helicopters (e.g. H225), ice protection systems are available, which are usually electrically operated and provide immediate heating in case of icing conditions. Due to the high energy requirements, it is difficult to transfer these technologies to small or medium-sized helicopters. In addition to simulation studies, experimental verifications in icing facilities are primarily used to design the required heating system. The disadvantage of conventional experiments is that rotational tests are largely not possible here, since most icing facilities are wind tunnels with comparatively small measurement cross sections. Rotational tests apply enormous centrifugal accelerations on the blade, which helps to deice faster and with less energy input. Rotational testing can therefore be used to determine the actual energy requirements of a de-icing system and optimize it for its use in helicopters.

As part of the InTEnt-H project, the whirl tower of the German Aerospace Center (DLR) in Brunswick was therefore converted into an icing test facility for rotors that is unique in Europe. Here, de-icing and anti-icing systems for rotor blades can be tested under centrifugal loads and various icing conditions.

2. ICING FACILITY

DLR's whirl tower is a very important rotor and blade test stand where new and blade-integrated systems can be investigated under centrifugal loads. The goal of the whirl tower conversion was to provide additional atmospheric conditions to investigate icing and de-icing of rotating rotor blades. In a first step, an insulated cooling chamber (light blue, Figure 1) was installed within the facility.

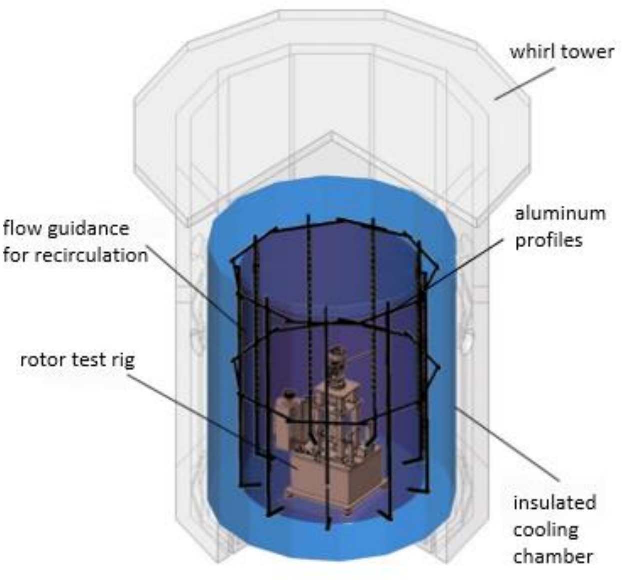

Figure 1: Sketch of DLR's whirl tower including icing facility

The cooling chamber is designed as a hexadecagon in order to be as circular as possible, has an interior diameter of about d_i = 5.3 *m*, and a height of h_i = 6.0 *m*. The walls and ceiling are made of sandwich panels consisting of a polyurethane rigid foam core of thickness h_{core} = 120 *mm* and stainless steel sheets ($h_{coating}$ = 0.7 *mm*) (Figure 2). At the floor, 2.5 *mm* thick V2A stainless steel plates were welded together, which ensures that the test stand can be entered even with heavy measuring equipment. Drains in the floor ensure that water can drain after the icing tests. A hatch in the ceiling still allows the use of the overhead crane.

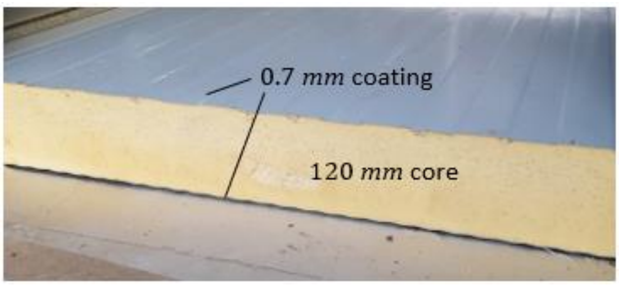

Figure 2: Section of a wall panel of the cooling chamber

In the cooling chamber, a flow guidance (dark blue, Figure 1) can be installed on aluminum profiles [1], which surrounds the test rig and enables the facility for a recirculating flow driven by the test stand's rotor. A conceptional drawing of the flow guidance, whose final design is currently still under development, is shown in Figure 3. It consists of a ballistic protection of stainless steel (dark blue) and hard plastic plates (grey). To protect the electrical components and to improve the flow, the entire rotor stand is encapsulated. This also minimizes the introduction of thermal energy from the electric motor into the cooling chamber.

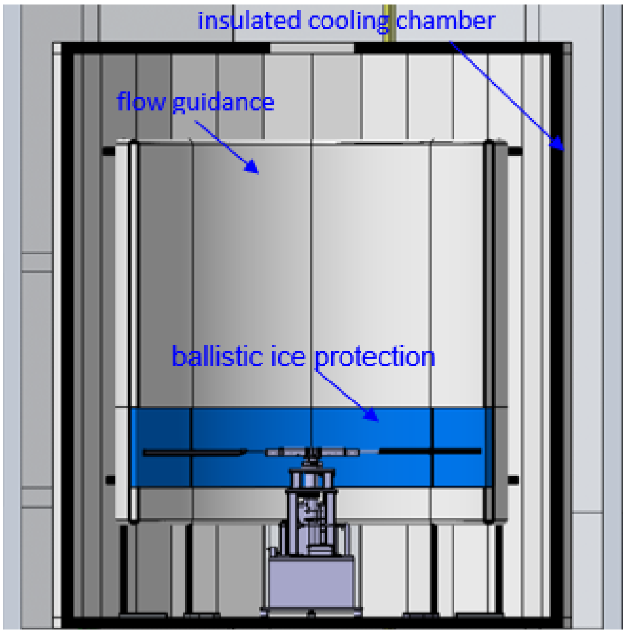

Figure 3: Concept of flow guidance within the cooling chamber

In order to obtain a first estimation of the flow conditions inside the cooling chamber, a CFD model was set up. Figure 4 shows the results of this very first simplified CFD calculation. The results are based on a 3D steady and non-viscous CFD calculation with a defined rotor downwash of approx. v_{CFD} = 10 *m/s*. In addition to the intended main circulation (blue) with core and outer flow, breakaway edges and areas with detached flow can be seen following the flow around the flow guidance (red), which indicates a possible accumulation of ice in these areas. Furthermore, due to the different flow velocities of core and outer flow, a static pressure gradient occurs over the flow path, which has to be considered when choosing a suitable planking. A strong vortex phenomena (purple) can be observed at the blade roots. The effect of a corresponding tip vortex (orange) is small compared to the vortex at the root. Another effect is the large swirl region located at the centre area (green) of the chambers ceiling. This can have a strong constricting effect (yellow) on the air coming from the outside stream. Particular attention must be paid to this area, since the nozzles for injecting the water-air mixture for ice formation are located here. Finally, it must be ensured that the intended area of the rotor plane is sufficiently wetted with water droplets.

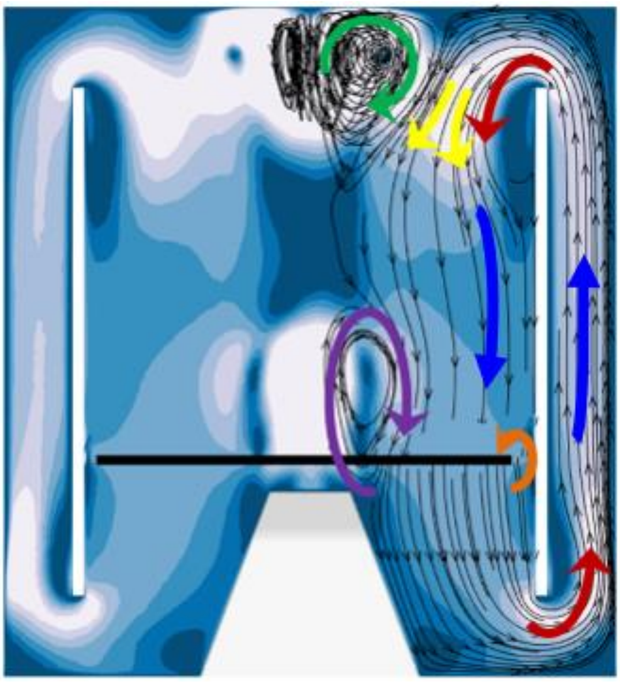

Figure 4: 3D CFD results show flow phenomena to be expected: blade tip vortex (orange), vortex separation areas (red), root backflow (purple), central ceiling vortex (green), and resulting flow constriction (yellow)

These simplified calculations provided a first impression of the phenomena to be expected. In the first test phases, the real flow conditions were then verified, especially in the area of the rotor plane, by using wool threads and numerous video cameras. Figure 5 shows the installation of the flow guidance installed in the cooling chamber. Since the quality of the icing conditions strongly depends on the flow quality, the dependence of the flow guidance radius on the homogeneity of the flow in the rotor area was to be investigated here in particular. However, the first icing tests already showed uniform icing even without flow guidance, so the further icing tests in the project were carried out without the planned flow guidance. This considerably simplified the execution of the tests and the maintenance of the test rig.

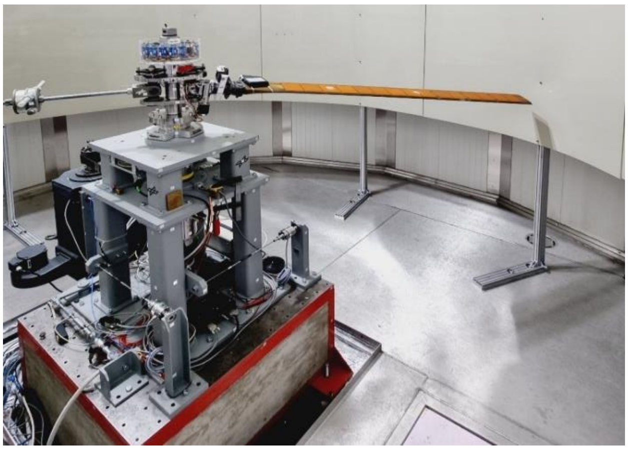

Figure 5: Test stand including the flow guidance

To protect the rotor test rig and its components from humidity , an enclosure made of thermal panels was designed and manufactured (Figure 6). The enclosure consists of a multi-part riveted construction framed with profiles, which is assembled in the center with clamping locks. A flexible sealing at the bottom of the cover ensures the movement of the rotor stand and prevents humidity from entering. Heat generated by the electric motor is not emitted into the cooling chamber by the enclosure, but can be conducted outside through the basement, thus significantly reducing the required cooling capacity.

Figure 6: Enclosure of rotor test rig, left: open, right: closed

To create a cloud of water droplets inside the cooling chamber, a ring with a radius of 1.35 *m* is installed below the ceiling of the chamber. This is attached to ropes and can be adjusted in height using pulleys attached to the ceiling. In the icing tests carried out so far, this was positioned at a distance of 1.3 *m* from the ceiling. 15 electrically heated and evenly distributed nozzles are attached to this spray ring (Figure 7). This system provides a water-air spray required for sufficient ice formation.

Figure 7: Installed spray ring system below the cooling chamber ceiling

A single nozzle DS55500 by "Spraying Systems Co." was tested under laboratory conditions for characterizing the spray by means of a Phase-Doppler-Interferometry (PDI) system. Based on interference patterns, such a system enables the determination of the spray droplet diameter and, derived from that, its liquid water content. The characterization is done by a variation of the parameters air and water pressure [2]. EASA CS29 Appendix C specifies the spray's liquid water content (LWC) and the median volume diameter (MVD) for continuous as well as for intermittent maximum conditions. The goal is to match the following demands:

$$MVD = 20\ \mu m$$

$$0.2\ g/m^3 < LWC_{contin.} < 0.8\ g/m^3$$

$$1.0\ g/m^3 < LWC_{intermitt.} < 2.5\ g/m^3$$

The overall concept of the test stand is shown in Figure 8 [3]. The spray ring system consists of 3 separate control circuits with 5 nozzles each. Preliminary tests have shown that controlling several nozzles connected in parallel results in the same injection quantities, so that grouping them together produces a valid injection pattern. The complexity of the control and regulation of the nozzles is thus significantly reduced.

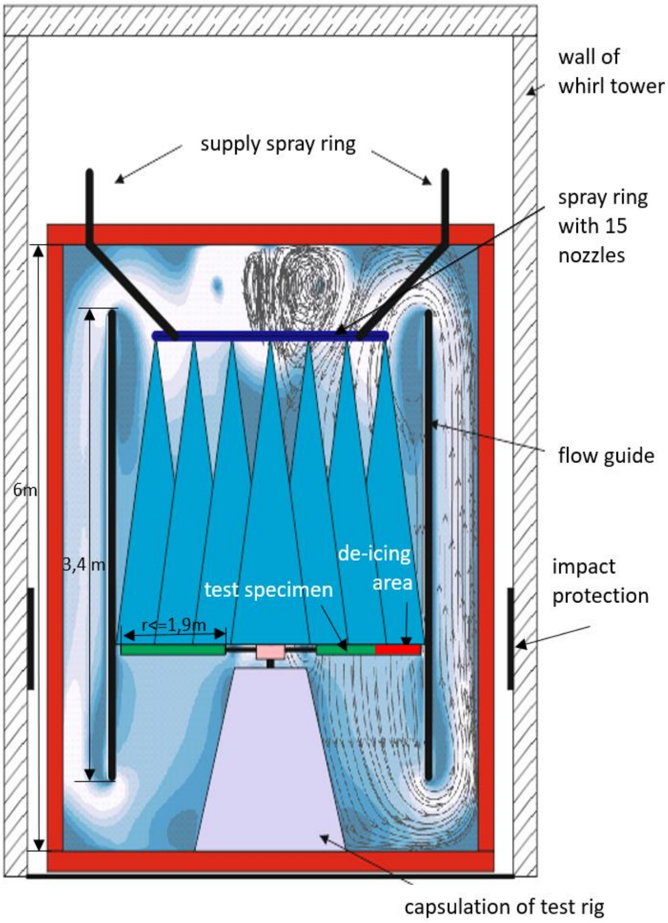

Figure 8: Overall test setup including the spray ring

Control air to switch the two-component nozzle on and off, compressed air and water are each fed through the ceiling by means of a hose package.

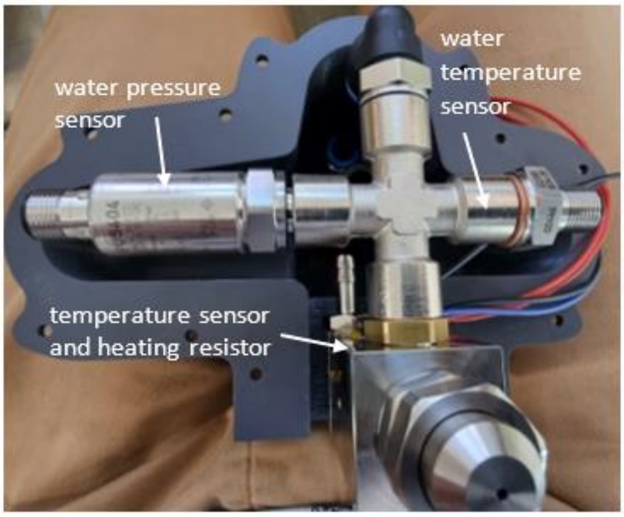

Figure 9: Internal structure of the nozzle assembly

On the cooling chamber roof there are numerous valves for controlling the compressed air and the water as well as measuring devices for various parameters of the fluids (Figure 10). In addition, water temperature and pressure are monitored individually at each nozzle (Figure 9) to ensure that injection conditions and thus injection rates are identical at each nozzle. This control is implemented and controlled on National Instruments (NI) hardware. The nozzles themselves are individually heated, just as the supply lines are insulated and heated to prevent freezing in the rotor tower.

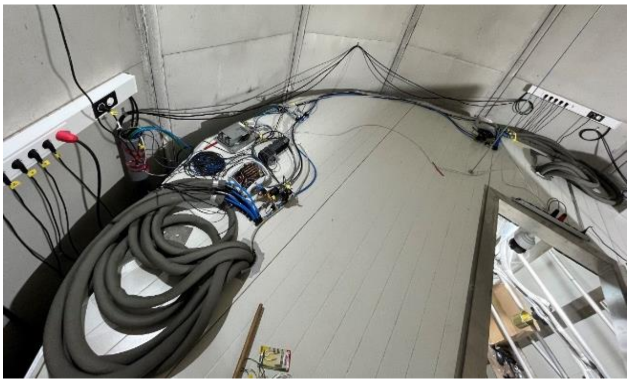

Figure 10: Cable routing, distribution box, NI system, power supply and control elements on the roof of the cooling chamber

The control parameters of the nozzles are the water pressure and the supply air pressure. By setting these parameters separately, the injection behavior of the nozzles can be varied for each control circuit. Regulation is possible for both pressures between 0 and 4 *bars* (limited by the maximum pressure of the nozzles). For each control circuit there are flow sensors for air and water, a pressure sensor for the supply air, and a pressure sensor for each nozzle as well as a temperature sensor for the water circuit. All signals are sent as analog signals to the FPGA module of the NI system and displayed graphically to the user on the interface.

A cooling unit provides atmospheric icing conditions. Due to its size, it is located outside the rotor tower.I It was necessary to connect a duct and chamber system to the cooling chamber in the outer area of the tower, made of the same material as the cooling chamber, housing the chiller and the fan. For reasons of sustainability, the cooling system operates with climate-neutral refrigerant CO_2 and has a cooling power of 50 *kW* in order to be able to realize temperatures below T = -20.0 *°C* during operation.

The setup of the icing facility is outlined in is outlined in Figure 11 and Figure 12.

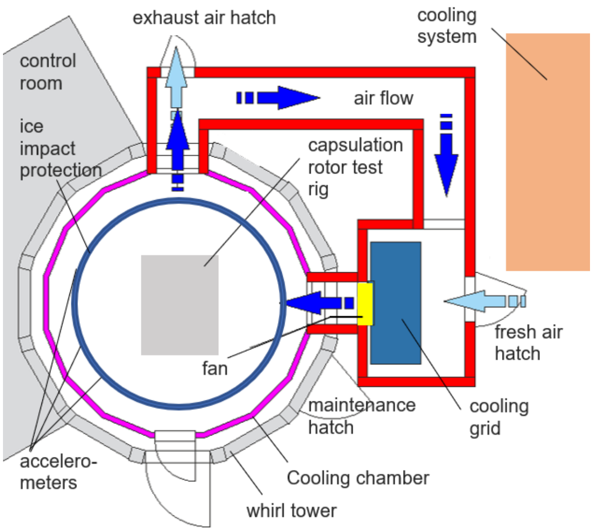

Figure 11: Cooling setup with built-in cooling chamber in the rotor tower - top view. incl. duct, chamber system, and cooling system

In cooling mode, when the hatches are closed, the fan of the radiator generates an air flow through the circular duct (Figure 13). The rotor in the center of the cooling chamber generates a circulation flow perpendicular to it during operation, so that there is complete mixing or homogeneous distribution of cold air throughout the facility. After the tests, an air exchange with the environment can be forced by opening the fresh air and exhaust air hatches with the help of the cooler fan (without cooling function) in order to support the drying process inside the cooling chamber after the water has drained off.

Figure 12: Components of the cooling system

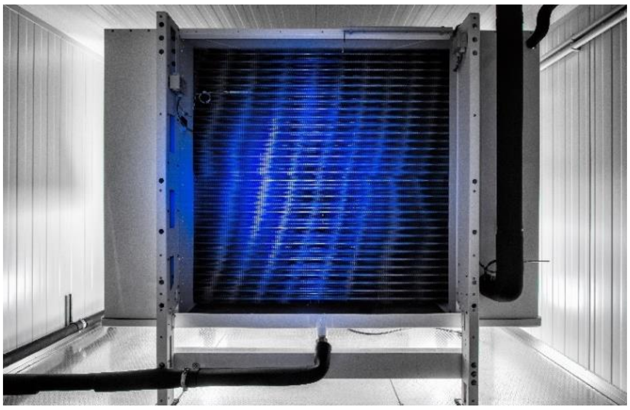

Figure 13: Chiller and fan behind it

3. WHIRL TOWER TEST RIG

The test rig configuration which was used for the first icing tests with rotating blades is shown in Figure 14. It was developed to meet different demands. In general, rotors with a radius of $0.8\,m < r < 2.5\,m$ can be tested in 2-blade or 1-blade configuration, in the latter case with an additional adjustable counter weight. The test stand is built from a solid steel structure to support radial loads of up to 150 *kN* in the rotating system. The structure is firmly bolted to a concrete block which rests on 4 pneumatically adjustable elastomeric buffers.

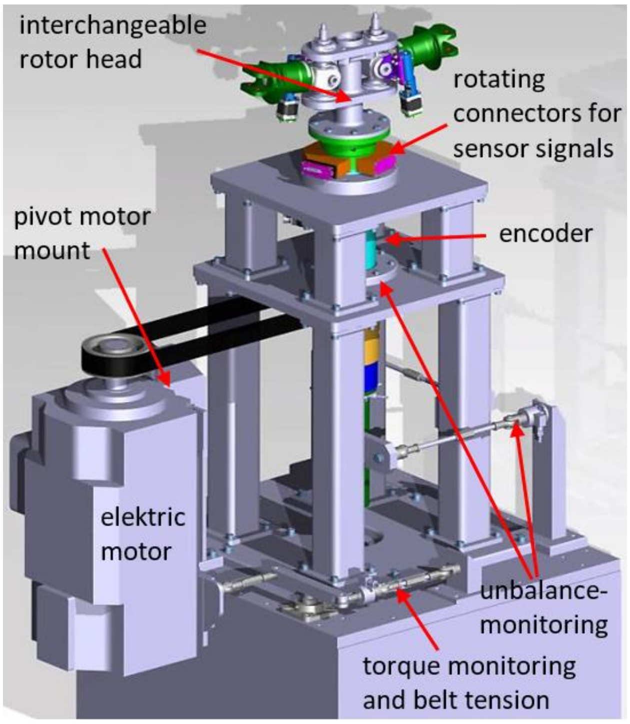

Figure 14: Components of the whirl tower test rig

The rotor shaft is driven by a 47 *kW* electric motor using a toothed belt. The torque as well as the occurring unbalance can be permanently monitored by various load cells and accelerometers. Furthermore, a slip ring system is integrated, which makes it possible to transmit numerous sensor data as well as high voltage signals. This can also be combined with a telemetry system. All data can be recorded with an external measurement acquisition system. The slip ring system has both pneumatic and hydraulic ports. Thus, compressed air and water-glycol related fluids with up to 10 bars can be transferred into the rotating system.

During the icing tests, unbalances will occur on the overall rotor due to different ice layer thicknesses on both sides of the rotor, which will lead to increased loads and must be monitored. For this purpose, an online display of the current imbalance situation has been developed.

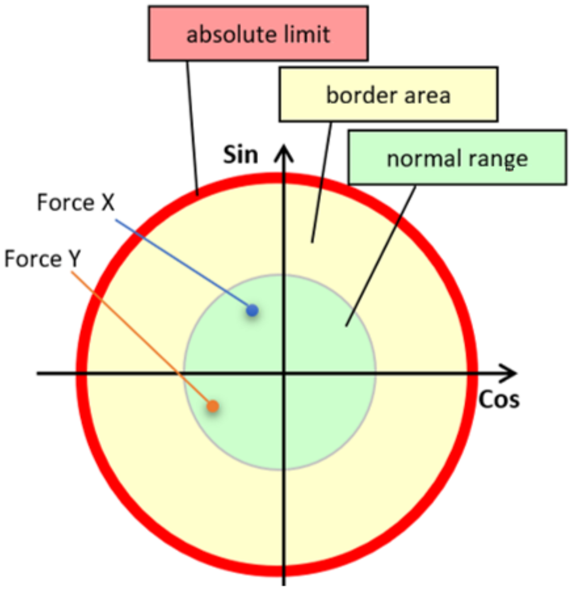

Figure 15: Polar diagram as basis for the unbalance plot

Due to the elastic bending of the rotor support structure during rotor imbalance, corresponding forces occur in the load cells and show a sinusoidal force curve as a result of the rotor rotation. Together with the azimuth position of the rotor, an unbalance plot (polar diagram, Figure 15) with 1/rev amplitude and phase and the respective normal and maximum values is generated from this, which is shown online on a display at the pilot station.

For testing de- and anti-icing systems, a special rotor hub system was developed to support two rotor blades with a radius of up to $r = 1.9\,m$. On one side an electric anti-icing system is installed to guarantee no icing on this rotor side. The other side is used to carry different de- or anti-icing technologies in the blade to test its performance. It is possible to adjust the radius of the blades from 1.75 *m* to 1.9 *m* when the rotor is stopped so that optimum flow conditions can be set. Furthermore, an adjustment of the angle of attack between -5° and +20° at standstill has been implemented, which corresponds to a common adjustment range of a helicopter rotor in real operation. The rotor is designed for a maximum rotational frequency of 78.5 *rad/s*, which follows from the maximum permissible unbalance of 3000 *N* caused by a one-sided ice buildup (ice thickness of 7.6 *mm* over 10*%* of the chord depth [4]). The maximum total thrust of 1500 *N*, which must also be considered, is associated with a corresponding rotor drive power, which heats up the rotor tower during operation. The maximum thrust is therefore limited by the power of the cooling system at minimum temperature. The rotor is operated in an environment with temperatures between -20 *°C* and +35 *°C* and is designed to be resistant to corrosion. Furthermore, there are options for balancing, mounting a camera for observing the leading edge of the test blade, and routing power, and fabric lines.

4. ICING AND DE-ICING RESULTS

After setting up the spray ring with the control technology and after some pre-tests, the injection was tested under icing conditions at -10°C. Various water-air mixture variations were tested. It was shown that the water-air mixture can be injected into the tower so that supercooled droplets are formed and ice formation takes place on the surfaces of the test blades. The first icing tests thus successfully demonstrated the functionality of the spray ring including control. After the successful initial icing tests, the first trials were carried out with a test body under icing conditions. These were carried out at low speed (300 rpm) in order to gain initial experience in the event of ice shedding and to avoid causing damage to the cooling chamber. The test body is made of aluminum and a 3D-printed contour body. Both the test body and the later used icing rotor have a chord length of *c* = 0.3 *m*, which is in the range of full-size blades of helicopters like H135 or H145. The aerodynamic effective span of the blade segments will be approximately *l* = 1.2 *m*, while the span of the de-/anti-icing technology towards the blade tip will be limited to about 0.5 *m*. The icing test with the test body showed the expected result (Figure 16 and Figure 17).The speed at which the icing took place also shows that the LWC at the icing location is in the right order of magnitude.

Figure 16: First icing tests in whirl tower, lower side of the test body

Figure 17 shows the icing on the test body, which exhibits rotor blade-typical ice formation. The ice nose at the leading edge had a thickness of about 30 *mm* at the blade tip after icing, corresponding to 10*%* of the blade depth, and half of that at the blade inner area. In terms of quantity, the rotor collected about 0.5 *l* of water per blade within less than 10 minutes.

Figure 17: Accumulation of ice at the leading edge of the test specimen

For the subsequent de-icing tests, a unique new 2-blade rotor system (Figure 18) was set up. This includes one blade with an electric foil heater for anti-icing (blade 1) and one with a fluid flow leading edge for anti-icing and de-icing (blade 2).

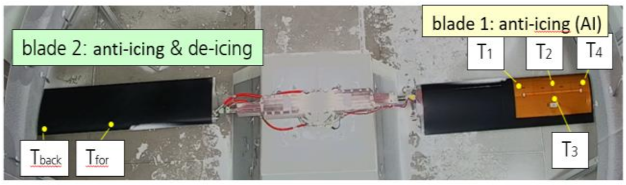

Figure 18: De-icing test in the whirl tower, de-icing blade (left) and reference blade (right)

The idea behind this implementation is to investigate alternative possibilities for energy-efficient de-icing of rotor blades. Here, one approach is to use waste heat, which is abundantly available and normally dissipated unused, from systems already installed in the helicopter for thermal de-icing of rotor blades. Such ideas are not new, but they have not yet been implemented in the rotorcraft sector. The novel aspect of the idea is tapping the gearbox oil as a heat source [5]. Here, the hot oil is fed through the hollow rotor mast into a heat exchanger in the rotor head where its thermal energy is transferred to a heating fluid in a closed heating circuit. The heat is then distributed through fluid pipes in the rotor blades along the leading edge of the blades by means of circulation pumps. In this test, the heated water-glycol mixture is only pumped through the outer leading edge area of blade 2. The electrical heating of blade 1 consists of 8 foil elements of the type Omega KHA510 with 4 elements each connected in series (one foil circuit). The maximum heat output for the sheet is just under 850 *W*.

During assembly, the rotor radius was set to 1.8 *m*, and the blade pitch angle was fixed at +8°. The maximum speed was initially limited to 450 *rpm* for safety reasons, corresponding to a blade tip speed of 85 *m/s*. The blades are instrumented with strain gauges and temperature sensors respectively. On blade 2, the temperature of the leading edge is recorded directly at the entrance to the fluid-flow leading edge ($T_{forward}$), and also the temperature of the trailing edge ($T_{backward}$) at the blade tip.

After the operational readiness of the technical systems was completed, the planned rotating test was carried out. On several test days, all systems were successfully put into operation and initial icing and de-icing tests were carried out with the new rotor (Figure 19). First, the rotor system was balanced by applying additional weights.

Figure 19: Different icing configurations during the first icing with the deicing blade, A: de-icing blade, A: de-icing blade , A: de-icing blade and reference

In several phases of cooling down between +20°*C* and -15°*C*, the cooling speed of the system could first be determined. In each case, the rotor was operated at 450 *rpm*. The average cooling rate is about 1.5 *K/min*, whereby higher gradients (1.7 to 2.0 *K/min*) can be achieved in the higher temperature range, as expected, and only about 1.0 to 1.5 *K/min* in the lower temperature range. Cooling down from +15°*C* to -10°*C* takes about 15 minutes.

For the final icing tests, the spray system was activated at 3 different temperatures for a specified period of time. The flow rate of the fluid-flowed blade 2 was stopped, while the anti-icing blade 1 was heated continuously with the maximum power of 800 *W*. An increase in unbalance and thus an ice formation on blade 2 was clearly visible in the sensors. Between the individual tests, both rotor blades were cleared of ice using hot air dryers. This allowed up to six icing runs to be carried out per day.

A visual comparison of the ice shapes obtained during the icing tests is shown in Figure 20 and Figure 21.

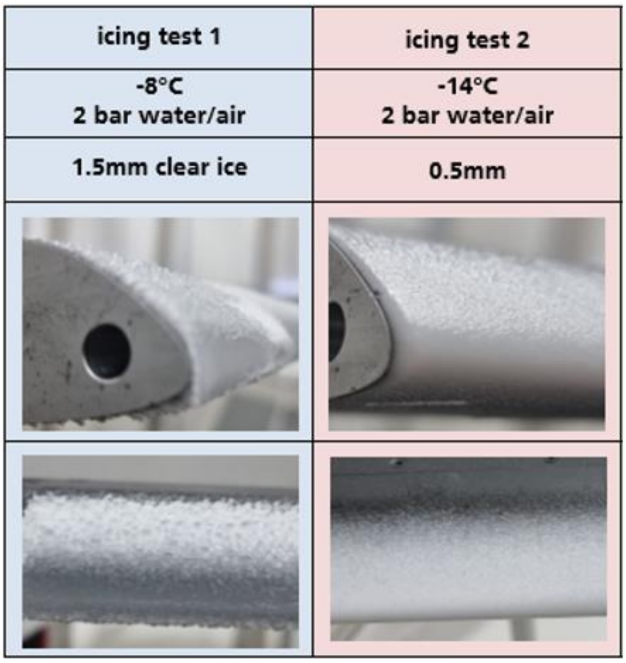

Figure 20: Ice formation on the rotating blade 2, icing at -8°*C* (left) and -14°*C* (right)

Depending on the icing parameters, different ice variations have occurred. Although far more factors influence the type of ice formation, in the first tests the focus is mainly on the cooling chamber temperature and the two pressures for the injected air-water mixture.

When icing at -8°*C*, the ice is rather transparent (clear ice) with a coarse structure and had a maximum thickness of about 1.5 *mm*. At -14°*C* the structure is much finer and it is now opaque and white with a maximum thickness of about 0.5 *mm*. When comparing the -20°*C* (see Figure 21) and -14°*C* ice forms, no significant difference can be seen. This also has a fine structure with a maximum thickness of about 1.0 *mm* and is opaque. As a further variation, in the fourth icing test, the air pressure of the spray nozzles was reduced to 1 *bar* instead of 2 *bars*, while the water pressure was still kept at 2 *bars*. The tests were performed at -20°*C*. The ice shape resembles that at -8°*C* with a rather coarse structure, but it is not transparent (rime ice).

After the last icing test at -20°*C*, the rotor was run up to 450 *rpm* again and then the pump of the de-icing system was switched on. The warm fluid from the tank is thus circulated towards the rotor blade. After reaching positive temperature values, the ice sheds from the blade.

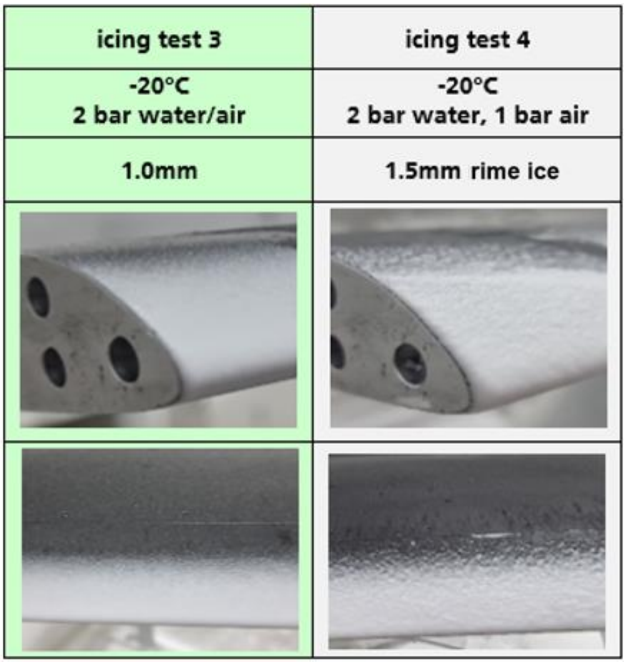

Figure 21: Ice formation on the rotating blade 2, icing at -20°*C* with 2 *bars* air pressure(left) and 1 *bar* air pressure (right)

The impact of the ice on the protection ring can be clearly identified by the accelerometers mounted on the back side of the protection ring (Figure 22). At the same time, there is an abrupt decrease in rotor unbalance.

Heating of the leading edge of blade 2 occurred relatively quickly, so it took no long time for the ice to chip off due to centrifugal force. As expected, the ice cracked off at the point where the warm liquid is supplied to the leading edge. In contrast, the ice still adhered to the inner part of the blade (Figure 23 and Figure 24). As can be seen in Figure 25, the ice protection ring successfully performed its function. It caught the ice immediately after it was chipped and ensured that the cooling chamber was protected from damage. The impact of the ice can be seen very clearly. The energy of the impact pulverized all the ice pieces, so no large pieces flew around and damaged the model.

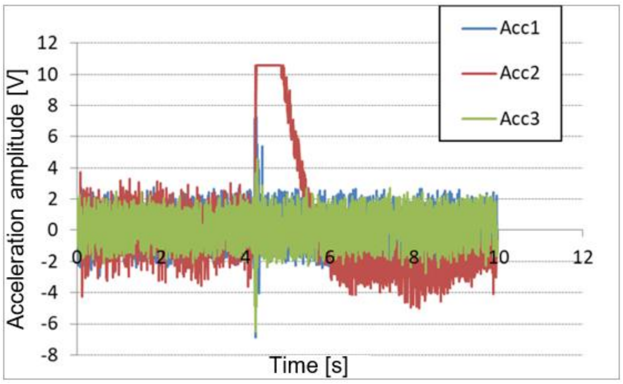

Figure 22: Moment of impact visible as accelerations during de-icing

Figure 23: Chipped ice on the leading edge of the test rotorblade

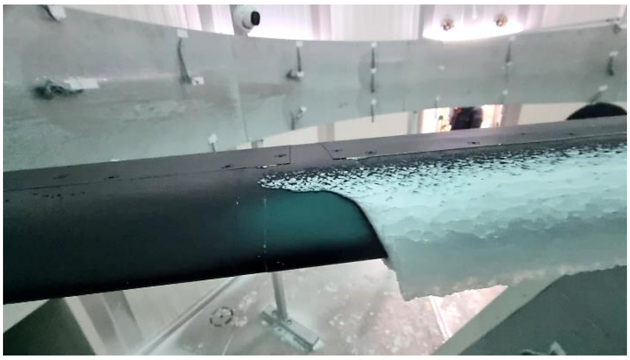

Figure 24: Chipped ice on the heated leading edge

Several tests confirmed the effectiveness of de-icing even with different icing configurations. Even though the waste heat system was not designed for de-icing, it was shown that it is also suitable for this purpose.

Figure 25: Impact mark from flaking ice on ice protection ring

Since this publication is only intended to give an overall view of the icing and de-icing activities within the InTEnt-H project, not all results can be discussed. A detailed description of the blade and rotor head design as well as a final evaluation of the results of all tests will be presented in later publications. Furthermore, the design and functionality of the sensor technology developed at DLR for the local detection of ice accretion will not be discussed here. This is another self-contained major topic and was also investigated in the context of the project. Reference is made to these publications [6] – [11]. Of particular interest is the investigation of the Lamb wave-based sensor technology within a conducted flight test in the project SENS4ICE [12].

5. Conclusions / Outlook

This paper gives an overall view of the new DLR icing facility and the icing and de-icing activities within the InTEnt-H project. The conversion of the rotor test rig into a highly modern and multi-purpose facility has been presented. The following steps have been addressed:

- installation of a cooling chamber
- layout of a flow guidance
- setup of a cooling system
- development of a spray ring system
- setup of the rotor test rig.

Furthermore, it was shown that various water-air mixtures could be successfully injected, causing different ice accumulations on the rotating rotor blade depending on the cooling chamber temperature. De-icing by means of electrical heating foils could be demonstrated just as successfully as de-icing by means of a heated fluid perfused leading edge.

The conversion of the rotor tower into a de-icing test stand for rotors provides DLR with a tool that is unique in Europe and will continue to be used in future projects. In the DLR internal project SAFER2, which started in January 2023, the de-icing test stand will be used, among other things, for the further development of sensor technology for ice detection for rotary system applications. At the same time, a characterization of the icing conditions with regard to the injected cloud of water droplets within the cooling chamber will be carried out in this context. Once the facility is fully operational and has demonstrated its capabilities, it will provide opportunities for a variety of subsequent icing and de-icing studies within the specifications of CS29 Appendix C. Because the facility has the capability to produce defined flow conditions with atmospheric icing conditions, the research is not limited to rotor blade applications. The area above the test stand is large enough to accommodate a variety of test specimens with or without aerospace engineering reference.

Author contact:

Steffen Kalow:	steffen.kalow@dlr.de
Rainer Bartels:	rainer.bartels@dlr.de
Oliver Schneider:	oliver.schneider@dlr.de
Dominic Sahyoun:	dominic.sahyoun@dlr.de
Ralf Keimer:	ralf.keimer@dlr.de

6. Acknowledgement

The InTEnt-H project has received funding from the Federal Ministry of Economic Affairs and Climate Action (BMWK) under the grant agreement number 20Y1702C.

Supported by:

Federal Ministry for Economic Affairs and Climate Action

on the basis of a decision by the German Bundestag

The SENS4ICE project has received funding from European Union's Horizon 2020 research and innovation program under grant agreement number 824253.

Horizon2020 European Union Funding for Research & Innovation

7. References

[1] Mendig, C., Schlemeier, N.: *„Entwurf und Detailkonstruktion einer Strömungsführung mit ballistischem Schutz und einer Tür."* Bachelorthesis. DLR- Internal Report. DLR-IB-FA-BS-2020-10, 70 S.

[2] Werner, J. Mendig, C.: *Lasermesssystem zur „Eisschichtdickenmessung an einem drehenden Rotorblatt im Vereisungsbetrieb des Rotorturms."* Bachelor thesis. DLR- Internal Report. DLR-IB-FA-BS-2020-157, 208 S.

[3] Hasani, V., Mendig, C.: *Detailkonstruktion, „Aufbau und Vortest einer Wassereinspritzeinrichtung für die Bereitstellung atmosphärischer Vereisungsbedingungen in einer Tiefkühlzelle"*. Masterthesis. DLR- Internal Report. DLR-IB-FA-BS-2020-155

[4] Yiqiang Han, Jose Luis Palacios and Edward C. Smith, *"An Experimental Correlation between Rotor Test and Wind Tunnel Ice Shapes on NACA 0012 Airfoils"*, SAE 2011 International Conference on Aircraft and Engine Icing and Ground Deicing, DOI: 10.4271/2011-38-0092

[5] Bartels, R., Schneider, O., Keßler, C.: *„Vorrichtung mit einem Rotorblatt und einer Wärmequelle und Hubschrauber“*, Patent DE 10 2017 106 7744 A1, German Aerospace Center (DLR)

[6] Mendig, C., Endres, M., Sommerwerk, H., Riemenschneider, J., Monner, H.P.: *„Eiserkennung durch Körperschallwellen*“, German Aerospace Society - Lilienthal-Oberth e.V., Bonn, 2016

[7] Mendig, C.: *“Icing Wind Tunnel and Detection of the Formation of Icing by Heat Cristallization”*, SAE Technical Paper 2015-01-2143, 2015, DOI:10.4271/2015-01-2143.

[8] Mendig, C.: *„Verfahren und Vorrichtung zum Erkennen von Vereisung einer von einer Luftströmung angeströmten Oberfläche“*, Patent DE 10 2015 100 522, German Aerospace Center (DLR)

[9] Mendig, Christian und Riemenschneider, Johannes und Monner, Hans Peter und Vier, Leonard Johannes und Endres, Matthias und Sommerwerk, Hannah (2018), “*Ice detection by ultrasonic guided waves.”* CEAS Aeronautical Journal. Springer. DOI: 10.1007/s13272-018-0289-0 ISSN 1869-5590

[10] Pohl, Martin und Riemenschneider, Johannes und Feder, Julia (2023) *Lamb-wave and impedance based ice accretion sensing on airfoil structures.* SPIE Smart Structures + NDE 2023, 12.-16. März 2023, Los Angeles, USA

[11] Pohl, Martin, “*LILD - Local Ice Layer Detector.*“ In: SAE AC-9C Aircraft Icing Technology Committee Meeting #75. SAE AC-9C Fall 2021 Virtual Committee Meeting, 18.-22. Okt. 2021

[12] Pohl, Martin, “*Wind tunnel and flight testing of a lamb wave based ice accretion sensor.*” International Conference on Icing of Aircraft, Engines, and Structures, 20.-22. Jun 2023, Wien, Österreich.